POLITECNICO
MILANO 1863

Department of Aerospace Science and Technology
Orbital Mechanics Course
Academic Year 2023/2024

Interplanetary and Planetary Explorer Missions

Project Asteria - 2308

Francesco Ceglie - PC 10796659, MC 247289
Alessandro Massini - PC 10990413, MC 243670
Francesco Paolo - PC 10738374, MC 252494
Caterina Maria Irma Pilotto - PC 10764521, MC 242312

Abstract

The following report aims to present the preliminary mission analysis of both an Interplanetary and a Planetary Explorer Mission.

The first part illustrates the study done to design the transfer from the departure planet, Mars, to the arrival body, Venus, with a flyby at the intermediate planet, Earth. A solution based on the mission cost is proposed, considering mission constraints such as the earliest departure and latest arrival set by the launch provider, the systems engineering team, and the Agency's leadership.

The subsequent section delves into the Ground Track estimation and orbit analysis for a mission designed to conduct Earth observation. Initially, the Nominal Ground Track is analyzed, and an orbit modification is proposed to achieve a Repeating Ground Track, enhancing communication with the network of ground stations.

Further study explores the impact of Solar Radiation Pressure and J_2 perturbations on both the Nominal Ground Track and the evolution of Keplerian elements. Two distinct methods of propagation are employed to obtain the Keplerian elements: the equation of motion and the Gauss planetary equations. To validate the perturbed model, a comparative analysis is performed using real data of COSMOS 1729 obtained from NASA/JPL's HORIZONS [4], utilizing TLEs sourced from Space-Track [5].

Contents

1 Interplanetary explorer mission

1.1 Introduction

The objective of the study is to design an interplanetary mission arriving on Venus and departing from Mars with an intermediate powered gravity assist on Earth. The earliest departure date from Mars and the latest arrival date on Venus are shown in Table 1. The figure of merit for the mission analysis is the total cost of the transfer, considering the initial and final heliocentric orbits of the departure and arrival planets as initial and final orbits of the spacecraft. The analysis is performed using the patched conics method, and the two interplanetary heliocentric arcs are obtained solving the Lambert's problem.

Earliest departure date	01/01/2028
Latest arrival date	01/01/2058

Table 1: Time constraints

1.2 Preliminary analysis of the time windows

The preliminary study aims to find a reasonable restriction of the departure, powered flyby, and arrival time windows to start the mission analysis. The estimation is done by computing the ΔV_{dep}, from Mars orbit to the first Lambert arc, and the ΔV_{arr}, from the second Lambert arc to Venus orbit, in the time window assigned with a coarse discretization. The values obtained are plotted in two contour plots as illustrated in Figure 1, the images display only the values of ΔV under 8 km/s to better visualize the region of minimization.

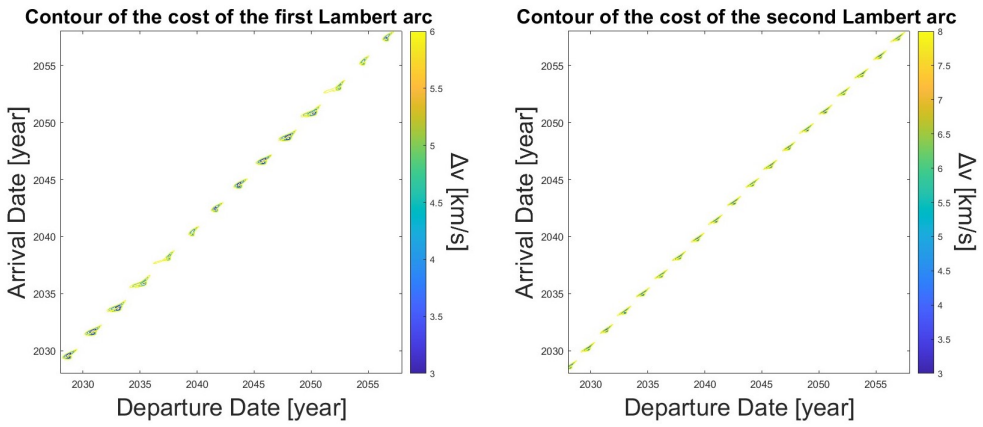

Figure 1: Contour plot of ΔV_{dep} and ΔV_{arr}

The repetition patterns in the contour plots are due to the Mars-Earth and Earth-Venus synodic periods. A first estimation of these parameters can be computed through Equation 1, where T_1 and T_2 are the orbit periods of the relative celestial object, considering the planet orbits as circular and coplanar [1]. The results are illustrated in Table 2.

$$T_{syn} = \frac{T_1 T_2}{|T_1 - T_2|} \tag{1}$$

	Earth	Venus
Mars	2.1353 years	-
Earth	-	1.5987 years

Table 2: Synodic Periods

To obtain the preliminary time windows, as shown in Table 3, since the regions of minimum are similar, the first available one is taken from the first graph and then a consecutive region is chosen from the second one. The selected regions respect reasonable minimum required times of flight of the Lambert arcs: seven months for the first transfer and four months for the second one.

Departure window	01/04/2028	01/10/2028
Flyby window	01/05/2029	01/09/2029
Arrival window	01/02/2030	01/07/2030

Table 3: Initial time windows

1.3 Mission Analysis

After defining the initial time windows through a coarse discretization, a multi-step approach is implemented, where each iteration refines the grid in the neighborhood of the dates of the minimum total cost of the mission identified in the previous step.

Therefore, for each refinement of the grid, a matrix of ΔV_{tot} is obtained and the minimum value is retrieved with its corresponding dates. The grid search is done over the three degrees of freedom: departure, flyby, and arrival windows, using three nested loops.

The total cost of the mission ΔV_{tot} is defined as the summation of ΔV_{dep}, Δv_p and ΔV_{arr}, where Δv_p is the impulse, tangent to the trajectory, that takes place at the common pericentre of the two different hyperbolic arcs of the powered flyby. Its magnitude is equal to the absolute value of the difference of the velocities of each arc at the intersection [3].

$$\Delta v_p = |v_p^- - v_p^+| \tag{2}$$

To find a physically valid solution a constraint is introduced on the magnitude of r_p of the flyby: the pericentre radius has to be higher than 1000 km from the Earth's surface, to keep the atmospheric drag force negligible. The nominal density at that altitude, according to the Exponential Atmospheric Model, is, in fact, equal to 3.019 x 10^{-15} kg/m^3 [3].

$$r_p > R_\oplus + h_{atm} \tag{3}$$

At the same time r_p needs to be lower than the radius of the Earth Sphere of Influence, to be consistent with the assumption of the patched conics method.

$$r_p < r_{SOI_\oplus} \tag{4}$$

The characteristics of the powered gravity assist are uniquely defined by solving Equation 5 once the incoming and outgoing heliocentric arcs are determined [3].

$$\delta = f(r_p, v_\infty^-, v_\infty^+) = \frac{\delta^-}{2} + \frac{\delta^+}{2} \tag{5}$$

where δ is the total turn angle of the powered flyby and δ^{-+} and v_∞^{-+} are respectively the turn angle and the excess velocity of the incoming and outgoing hyperbole.

1.4 Final trajectory

The selected interplanetary transfer has a ΔV_{tot} equal to 6.7481 km/s. The characteristics of this transfer, in terms of heliocentric arcs and powered gravity assist, are presented in the following sections.

1.4.1 Heliocentric arcs

The heliocentric arcs of the optimal solution take place in the dates displayed in Table 4 and are characterized by the Keplerian elements in Table 5.

	Date	Time
Departure	08/09/2028	23:18:24
Flyby	14/08/2029	03:03:06
Arrival	26/02/2030	06:43:29

Table 4: Final dates

	a[km]	e[-]	i[deg]	Ω[deg]	ω[deg]	θ[deg]
First arc	194681596	0.2373	1.90	321.64	333.50	161.35 - 26.50
Second arc	131725771	0.1870	4.31	141.64	30.46	149.54 - 16.58

Table 5: Keplerian elements

Figure 2 shows the heliocentric trajectory, the orbits of the planets involved, and the relative positions of the celestial objects at departure, flyby and arrival.

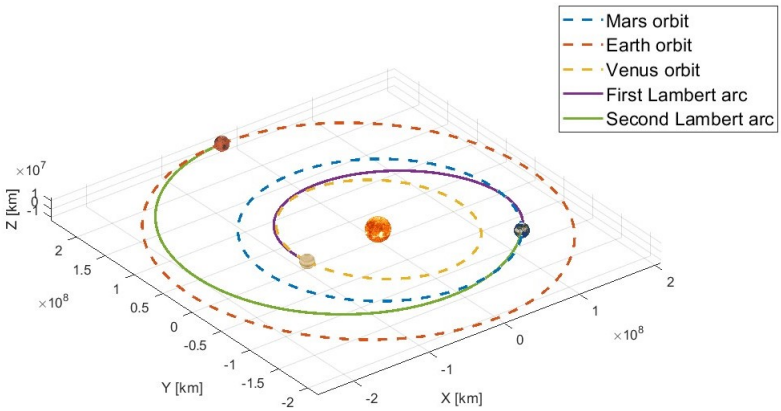

Figure 2: Lambert arcs

Due to the shape of the Lambert arcs and their ranges of true anomaly values, shown in Table 5, the values of ΔV_{dep}, ΔV_{arr} and times of flight (TOF) are compared with the ones of a hypothetical Hohmann transfer case.

To perform the computation, in the Hohmann arcs case, the planet orbits are considered coplanar and circular with a radius equal to the one that the planets have in the optimal date found. The results obtained are shown in Table 6.

Arc	ΔV_{dep}[km/s]	TOF[s]		Arc	ΔV_{arr}[km/s]	TOF[s]
First Lambert	2.4817	29303082		Second Lambert	4.2664	16947623
First Hohmann	2.7636	23351124		Second Hohmann	2.8437	12734211

Table 6: Comparison between Lambert arcs and Hohmann arcs

Both the first and the second Lambert arcs are similar to the corresponding case of the Hohmann transfer in terms of TOF. Meanwhile, only the first arc is comparable to the Hohmann arc in terms of the cost of the impulse maneuver. This is likely because, to minimize the overall cost of the mission, a trade-off between the individual costs of the two Lambert arcs has to be done.

1.4.2 Powered gravity assist

Given the radius of the Sphere of Influence of the Earth and the excess velocity of the incoming and outgoing hyperbole, obtained by the definition of the two heliocentric arcs, it is possible to characterize the flyby of the optimal solution through the data listed in Table 7. Δv_{flyby} is the magnitude of difference between the excess velocity vectors and Δt_{flyby} is the total time required to perform the flyby.

$r_p[km]$	$\delta[deg]$	$\Delta v_p[km/s]$	$\Delta v_{flyby}[km/s]$	$v_\infty^-/v_\infty^+[-]$	$\Delta t_{flyby}[s]$
8403.88	87.53	$7.967\text{x}10^{-11}$	6.3606	1.00	380634.37

Table 7: Flyby data

From the value of Δv_p it is possible to conclude that the powered gravity assist can be considered as a purely ballistic flyby. This statement can also be verified through the values of the magnitude of the two excess velocities, which are almost equal as shown in Table 7.

It is also important to highlight the difference in the order of magnitude of Δv_p and Δv_{flyby} which indicates that the flyby is advantageous: Δv_{flyby} represents the increase of the heliocentric velocity due to the maneuver.

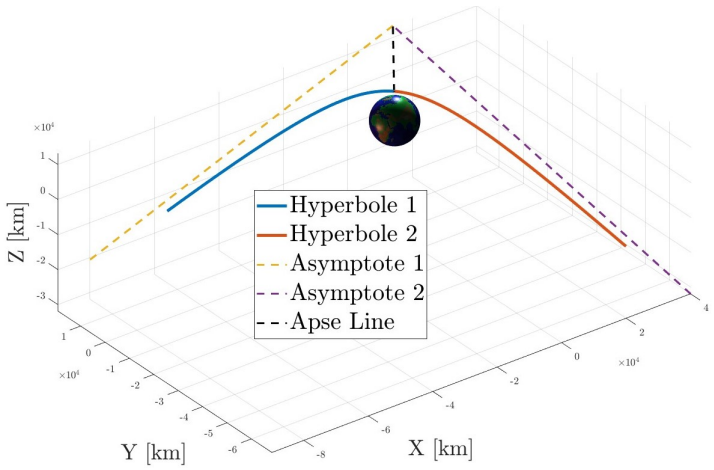

Figure 3: Flyby

2 Planetary explorer mission

2.1 Introduction

The main goal of the study is to analyze and estimate the Ground Track of an assigned orbit.

The first analysis is conducted on an unperturbed orbit. Then, a modification of it is proposed to obtain a Repeating Ground Track to guarantee better communications with the network of ground stations.

Afterwards, the focus is shifted to the effects of two orbit perturbations: the J2 and the Solar Radiation Pressure (SRP). The influence of these is studied in terms of the alteration of the Ground Track and the evolution of the Keplerian elements with respect to the unperturbed case.

2.2 Nominal orbit data

The initial Keplerian elements of the orbit are stated in Table 8.

$a[km]$	$e[-]$	$i[deg]$	$\Omega[deg]$	$\omega[deg]$	$\theta_0[deg]$
26539	0.5557	71.7849	90	45	0

Table 8: Nominal Keplerian Elements

From them it is possible to obtain the values of the pericentre and apocentre radii:

- $r_p = 11791\ km$
- $r_a = 41287\ km$

The Drag effects at these altitudes can be neglected, therefore the dominant perturbations are the Gravitational, the Solar Radiation Pressure, and the Third-Body ones. In the following analysis, only the first two are considered.

2.3 Unperturbed Ground Tracks

2.3.1 Nominal Ground Track

The Ground Track is defined as the projection of a satellite's orbit onto the Earth's surface [1]. Therefore, as the spacecraft moves along its orbit, its trace on Earth's surface is defined by latitude ϕ and longitude λ values.

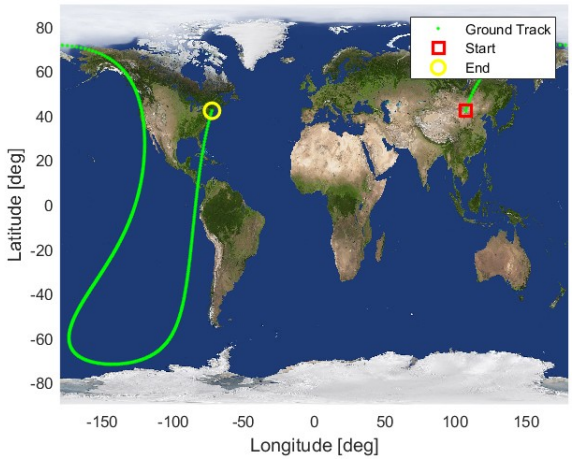

Figure 4: One period propagation

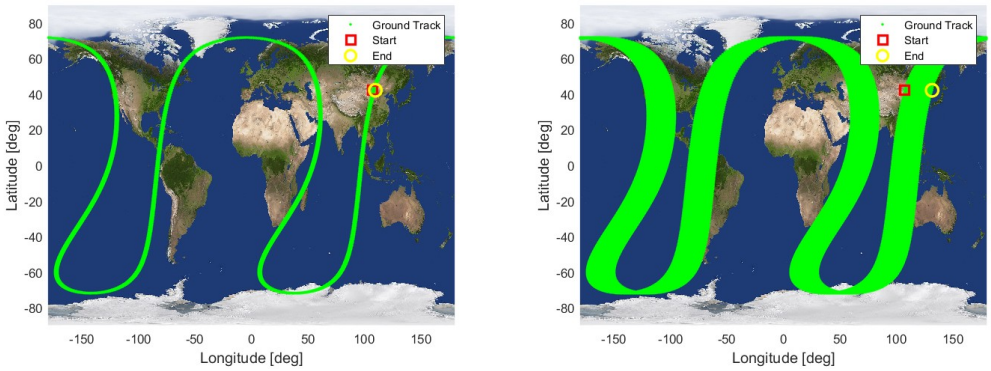

Figure 5: Ten and One hundred periods propagations

While the spacecraft is orbiting, the Earth's rotation around its axis causes a westward advancement of ground track: after one orbital period the longitude drifts following Equation 6.

$$\lambda = \lambda_0 - \omega_\oplus T \tag{6}$$

Where λ_0 is the initial longitude, $\omega_\oplus$ is the Earth's angular velocity, and T is the orbital period of the spacecraft.

Although the propagated Ground Track for ten periods seems to return to its initial point, since the orbital period is nearly half the period of the Earth's rotation, by propagating the orbit for one hundred periods the non-repetition is evident. This leads to problems with ground stations communications, which can not always be performed. A possible solution is computing a Repeating Ground Track.

2.3.2 Repeating Ground Track

A Repeating Ground Track can be achieved by modifying the orbital period T, and consequently the semi-major axis a of the orbit, in such a way that the Ground Track will repeat itself after k satellite revolutions and m Earth rotations.

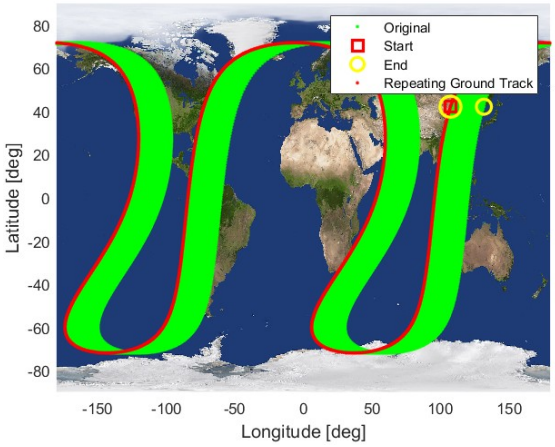

Figure 6: Repeating Ground Track and Nominal Ground Track propagated for one hundred periods

The result is obtained through the following equations:

$$T = \frac{m}{k} T_\oplus \tag{7}$$

$$a = \sqrt[3]{\frac{\mu_\oplus T^2}{4\pi^2}} \tag{8}$$

where $\mu_\oplus$ and $T_\oplus$ are the gravity constant and the rotation period of the Earth. Setting $m = 1$ and $k = 2$ a semi-major axis $a = 26563\ km$ is obtained.

As illustrated in Figure 6 with this relatively small modification it is possible to obtain a Ground Track that perfectly repeats itself for each multiple of m, k.

2.4 Analysis of the Perturbations

In order to have a more realistic model, orbit perturbations have to be taken into account. The two most significant considered ones, at nominal orbit altitude, are introduced by the J_2 effect and the Solar Radiation Pressure. To consider their effects, starting from the unperturbed two-body problem in Cartesian coordinates, the accelerations introduced by the two disturbances are added to the right-hand side of Equation 9.

$$\ddot{\boldsymbol{r}} = -\frac{\mu_\oplus}{r^3}\boldsymbol{r} + \boldsymbol{a_{J_2}} + \boldsymbol{a_{SRP}} \tag{9}$$

Alternatively, to find the time evolution of $\boldsymbol{r}$ and $\boldsymbol{v}$, the variation of orbital elements via the Gauss planetary equations can be evaluated. In this case, the accelerations need to be expressed in the *tnh* (Tangential - Normal - Out of plane) reference frame. Therefore, in this specific model, all of the perturbing accelerations are first computed in Cartesian frame and then rotated in the *tnh* one [1].

2.4.1 J_2 effect

The J_2 effect is caused by Earth oblateness and is a function of the geocentric distance r and the latitude ϕ [3].

The perturbing gravitational acceleration $\boldsymbol{a_{J_2}}$ can be expressed as illustrated in Equation 10.

$$\boldsymbol{a_{J2}} = \frac{3}{2}\frac{J_2\mu_\oplus R_\oplus^2}{r^4}\left[\frac{x}{r}\left(5\frac{z^2}{r^2}-1\right)\hat{\boldsymbol{i}} + \frac{y}{r}\left(5\frac{z^2}{r^2}-1\right)\hat{\boldsymbol{j}} + \frac{z}{r}\left(5\frac{z^2}{r^2}-3\right)\hat{\boldsymbol{k}}\right] \tag{10}$$

Its most relevant effects are the secular ones: the Nodal and the Perigee regression or precession, which respectively alter Ω and ω. The variation of these two elements depends on the value of the inclination and, since the nominal orbit has $63.4 < i < 90$, a regression of both RAAN and perigee anomaly is expected.

The other Keplerian elements a, e and i, under J_2 effect, show an oscillatory behavior around a fixed value with a one orbit period. Therefore their secular effects are null.

2.4.2 SRP effect

The Solar Radiation Pressure perturbation is due to Sun direct electromagnetic radiation that exerts a force on the spacecraft proportional to its cross surface [3]. The associated perturbing acceleration $\boldsymbol{a_{SRP}}$ can be expressed by Equation 11.

$$\boldsymbol{a_{SRP}} = -p_{SR@1AU}\frac{AU^2}{||\boldsymbol{r_{SC}}||^3}C_R\frac{A_{SC}}{m}\boldsymbol{r_{SC}} \tag{11}$$

Where AU is the Astronomical Unit, $p_{SR@1AU} = 4.5\times10^{-6}\ \frac{N}{m^2}$ is the Solar Radiation Pressure at $r = 1\ AU$, C_R is the radiation reflectivity coefficient, which depends on the optical properties of spacecraft surface, $\boldsymbol{r_{SC}}$ is the vector connecting the Sun center and the satellite, and $\frac{A_{SC}}{m}$ is the area-to-mass ratio relative to Sun direction. A_{SC} refers only to the spacecraft surface exposed to the Sun. The parameter values used in this model are $C_R = 1$, $\frac{A_{SC}}{m} = 5\,m^2/kg$. To find $\boldsymbol{r_{SC}}$, the Earth ephemeris has been used to obtain the position vector of the Earth with respect to the Sun and added the position vector of the spacecraft with respect to the Earth.

2.5 Perturbed Ground Track

Once the effects of the major perturbations are considered in the analysis it is possible to have a more realistic model of the Ground Track. In this case, the Cartesian formulation is used, as shown in Equation 9. The obtained results are illustrated in Figure 7.

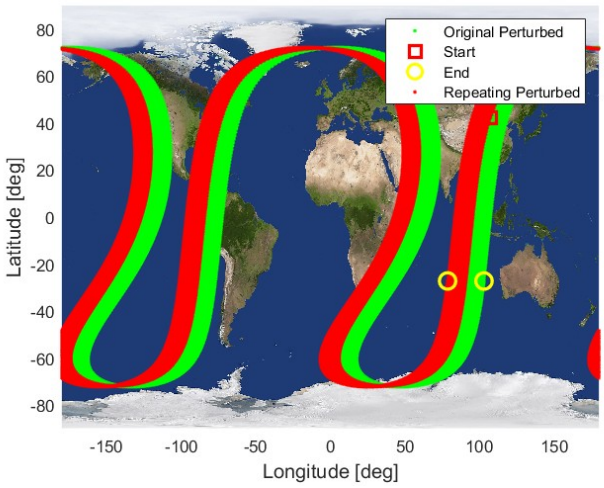

Figure 7: Nominal and Repeating Perturbed Ground Tracks propagated over one hundred periods

The previous figure shows how the semi-major axis variation computed through Equations 7 and 8 is no longer able to guarantee the repetition of the Ground Track. This phenomenon is bound to the presence of J_2 effect which introduces an additional westward drift of the ground track with respect to the unperturbed case, since it leads Ω to decrease. Furthermore, as side effect, it provides to a an oscillatory behavior around its nominal value.

Due to the same motivations, the Nominal Ground Track is also different with respect to the unperturbed case.

2.6 Evolution of Keplerian Elements

Given the nominal conditions for the orbit shown in Table 8 and the perturbing accelerations, the orbit is propagated for different time spans to analyze both short and long period effects. Results are then filtered with a low-pass filter to better visualize the secular effects of perturbations.

The propagation is carried out using both the Cartesian formulation and the Gauss planetary equations. To compare these two methods outcomes the relative errors between them then are computed.

The results are reported in Figure 8.

The short period J_2 effects are visible in the ten periods plots and consist in oscillations of all the Keplerian elements which have a period equal to the orbital one. Whereas its secular effects, noticeable in the ten years plots, produce, according to the nominal inclination, a decrease of the Right Ascension of the Ascending Node (RAAN) and the argument of perigee. It doesn't affect a, e, and i.

SRP contribution is particularly relevant for the inclination and the eccentricity, although in the ten years plots it can be noticed an annual quasi-periodicity of every orbital element [2]. The one-period effects of SRP aren't easily visible because influenced by the J2 ones.

Therefore, over ten years, as illustrated in Figure 8, a remains constant on average even though presenting periodical oscillations, e and i have a highly oscillatory behavior due to the Solar Radiation Pressure and, finally, Ω and ω have a decreasing secular behavior caused by J_2 and some slight annual oscillations caused by the SRP.

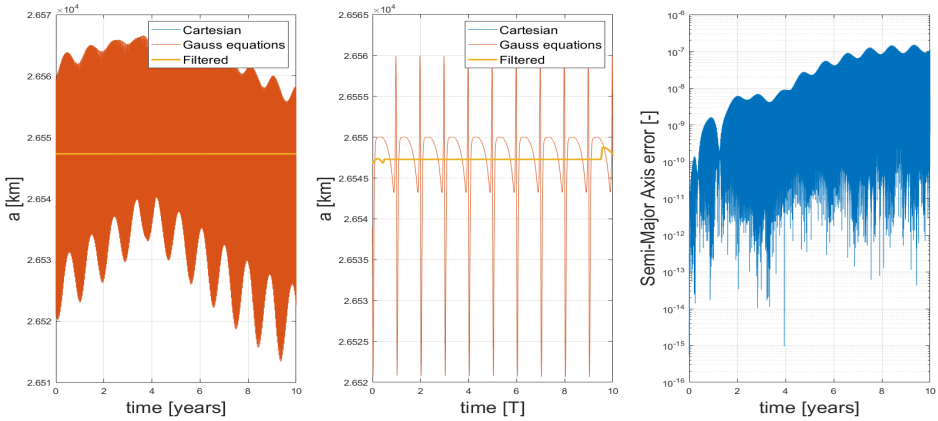

(a) Semi-Major axis

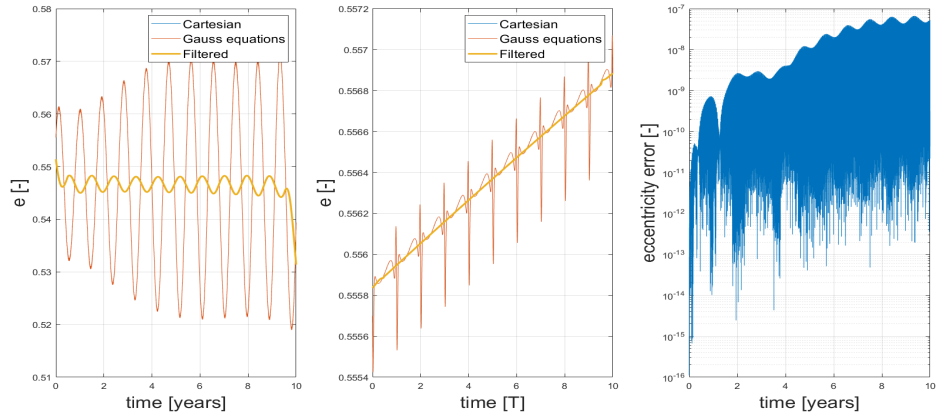

(b) Eccentricity

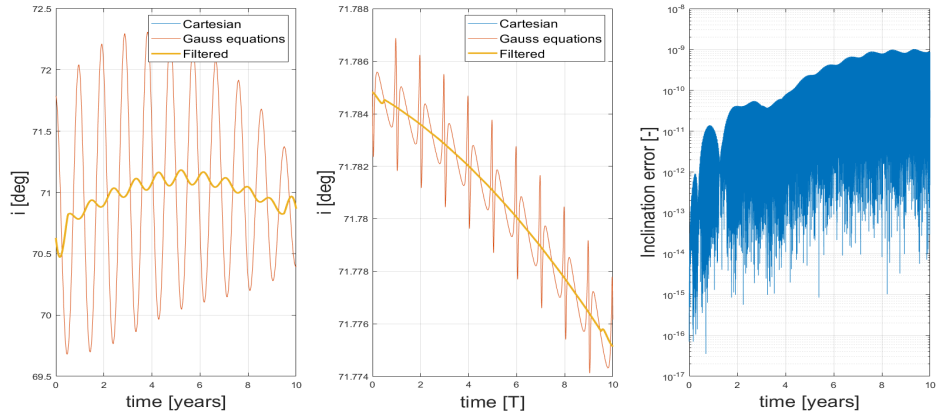

(c) Inclination

Figure 8: Keplerian elements evolution evaluated for ten years and ten periods and relative errors

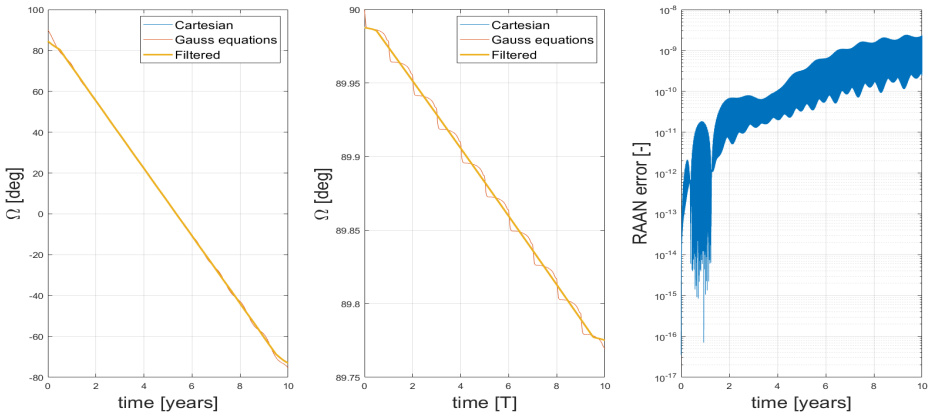

(d) Right Ascension of the Ascending Node

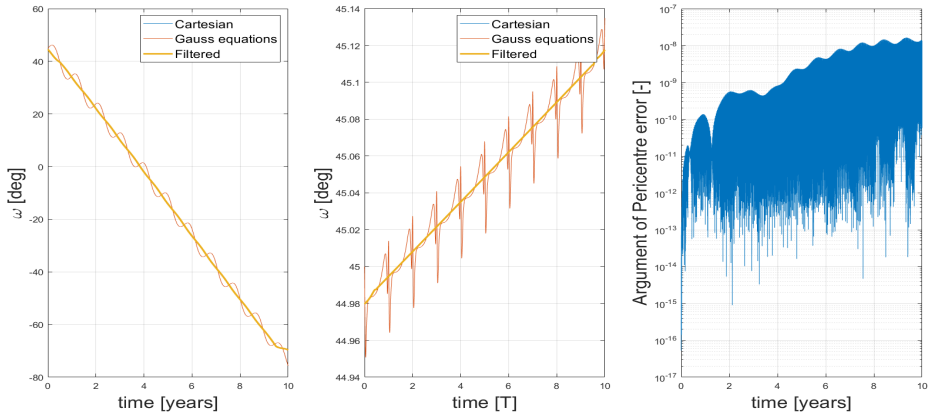

(e) Argument of perigee

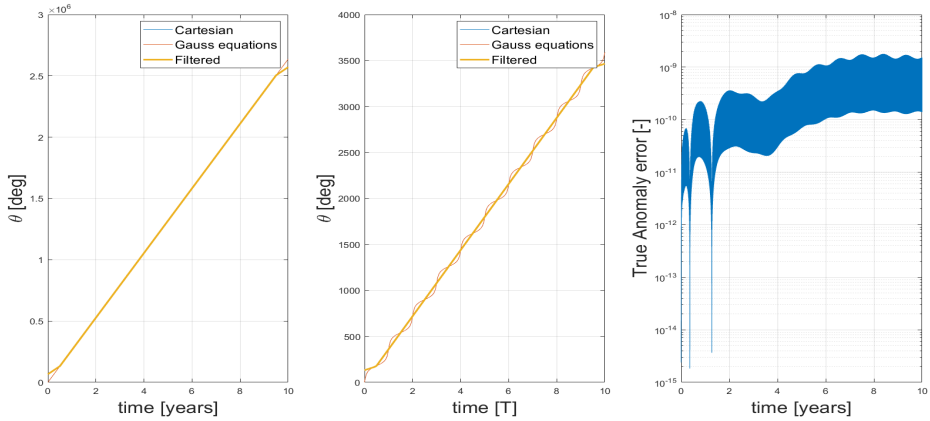

(f) True Anomaly

Figure 8: Keplerian elements evolution evaluated for ten years and ten periods and relative errors

The third column of Figure 8 shows that none of the relative errors between the two methods exceeds an order of magnitude of 10^{-7} after ten years of propagation.

The computational costs of the two methods, expressed in terms of time required to run a ten years propagation using 10000 equally spaced points, are reported in Table 9. The two methods resulted to be quite similar from this point of view.

Gauss planetary equation	$126s$
Cartesian formulation	$120s$

Table 9: Elapsed Time

Figure 9 shows the perturbed orbit after one year of propagation. From Figure 9a the westward rotation of the ascending node is clearly visible, while from Figure 9b it is possible to see that a and e are not fixed.

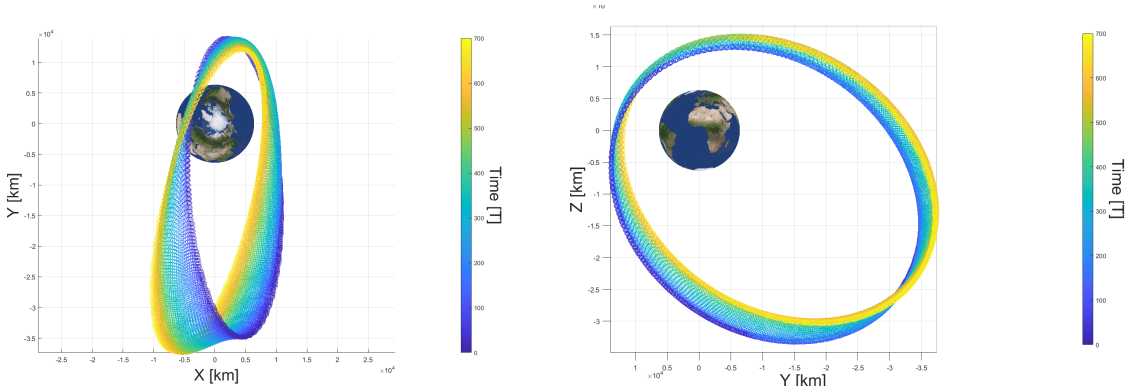

(a) $X - Y$ plane (b) $Y - Z$ plane

Figure 9: Perturbed orbit over one year

2.7 Comparison with real data

As an additional validation of the implemented model, it is possible to make a comparison with the data coming from a real in-orbit satellite. Therefore, an object which operates in the same orbital region as the analyzed Planetary Explorer is chosen.

For this study, the satellite COSMOS 1729 is selected. The real Keplerian elements that describe its orbit from 01/01/2000 to 01/01/2001 are retrieved from NASA/JPL's HORIZONS [4] by using the TLEs taken from Space-Track [5].

The orbital elements of COSMOS 1729 on 01/01/2000, shown in Table 10, are then propagated using the model, which considers only the two perturbations previously presented.

$a[km]$	$e[-]$	$i[deg]$	$\Omega[deg]$	$\omega[deg]$	$\theta_0[deg]$
26551	0.5118	68.1348	259.03	279.43	201.58

Table 10: Keplerian Elements of COSMOS 1729 on 01/01/2001

In Figure 10 are shown the results of the comparison.

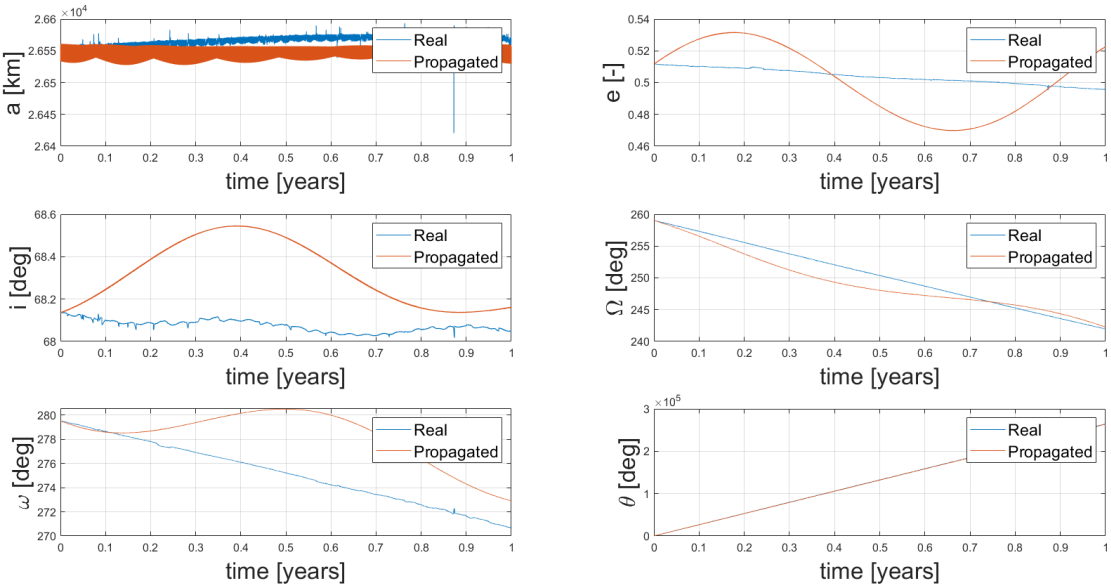

Figure 10: COSMOS 1729 Keplerian elements evolution

From Figures 8 and 10, it is possible to notice that, as expected, the evolutions of the propagated data for COSMOS 1729 orbit and the previously analyzed ones are similar.

On the other hand, the eccentricity and the inclination computed by the model are slightly different from the ones extracted from the ephemerides of the real spacecraft.

This can be attributed to the fact that this specific model does not take into account other types of disturbances to which the satellite is subjected instead. For instance, the Third Body perturbation has secular effects on e, i, and ω. Moreover, the satellite performs impulsive maneuvers to maintain the desired orbit [3].

As further evidence the real elements behavior is non periodic and, mostly for a and i, it has some impulsive changes which are impossible to predict by the implemented model.

Despite this, even if the model does not consider all the possible factors influencing the orbit, it can be considered as a good tool to conduct a preliminary analysis of an Earth-centered orbit with those specific characteristics.

References

[1] Howard D. Curtis, *Orbital Mechanics for Engineering Students*, Butterworth-Heinemann, September 2020

[2] David A. Vallado, *Fundamentals of Astrodynamics and Applications*, McGraw-Hill Primis Custom Pub, January 1997

[3] Camilla Colombo, *Orbital Mechanics Course Notes*, Politecnico di Milano, 2023

[4] Nasa/JPL's horizons, https://ssd.jpl.nasa.gov/horizons/app.html

[5] Space-Track, https://www.space-track.org/